Journal of Fluorine Chemistry 130 (2009) 67–73

Contents lists available at ScienceDirect

Journal of Fluorine Chemistry

journal homepage: www.elsevier.com/locate/fluor

Materials corrosion in molten LiF–NaF–KF salt

Luke C. Olson *, James W. Ambrosek, Kumar Sridharan, Mark H. Anderson, Todd R. Allen

Department of Engineering Physics, 1500 Engineering Drive, University of Wisconsin-Madison, Madison, WI 53706, USA

ARTICLE INFO

Article history:
Received 17 March 2008
Received in revised form 6 May 2008
Accepted 11 May 2008
Available online 16 May 2008

Keywords:
FLiNaK
Molten salt
Fluorides
Corrosion
Materials

ABSTRACT

Corrosion tests of high temperature alloys, Hastelloy-N, Hastelloy-X, Haynes-230, Inconel-617, and Incoloy-800H were performed in molten fluoride salt, FLiNaK (LiF–NaF–KF:46.5–11.5–42 mol%) with the goal of understanding the corrosion mechanisms and ranking these alloys for their suitability for molten fluoride salt heat exchanger and thermal storage applications. The tests were performed at 850 °C for 500 h in sealed graphite crucibles under an argon cover gas. Corrosion was noted to occur predominantly by dealloying of Cr from the alloys, an effect that was particularly pronounced at the grain boundaries of these alloys. Weight-loss due to corrosion generally correlated with the initial Cr-content of the alloys, and was consistent with the Cr-content measured in the salts after corrosion tests. Two Cr-free alloys, Ni-201 and Nb–1Zr, were also tested. Ni-201, a nearly pure Ni alloy with minor alloying additions, exhibited good resistance to corrosion, whereas Nb–1Zr alloy exhibited extensive corrosion attack. The graphite crucible may have accelerated the corrosion process by promoting the formation of carbide phases on the walls of the test crucibles, but did not alter the basic corrosion mechanism.

1. Introduction

Molten fluoride salts have been proposed for use as primary reactor coolants, media for transfer of high temperature process heat from nuclear reactors to hydrogen production facilities [1], for solar thermal energy storage [2], and as a means to raise heat-to-electricity conversion efficiencies of solar power towers to about 50% [3]. These salts are characterized by high thermal conductivities, high specific heats, low viscosities, and high boiling points. Materials corrosion has however been recognized as an issue in molten fluoride salts. In most high temperature industrial environments, materials derive their corrosion resistance from the formation of a protective surface film of an oxide of Cr, Al, or Si; elements that are added to the base alloy [4,5]. In molten fluoride salts these passive oxide films are chemically unstable, and corrosion is driven largely by the thermodynamically driven dissolution of alloying elements into the molten salt environment [6,7]. An understanding of molten fluorides' tendency to remove elemental constituents from an alloy can be achieved from phase diagrams, acid–base effects, and the redox potential of the system [8].

The free energy of formation of fluorides can be used to determine the most stable fluoride compounds in the melt formed by the alloying elements and these elements can be expected to be selectively attacked [8]. A National Aeronautic and Space Administration (NASA) study [2] determined that the tendency for common alloying constituents to corrode in molten fluoride salts increased in the following order: Ni, Co, Fe, Cr, Al. This is supported by Gibb's free energy of formation of various fluorides shown in Fig. 1. The same study [2] determined that refractory metals Nb, Mo, and W could be expected to be relatively free from attack. Based on this analysis, a Mo-containing Ni-based alloy, such as Hastelloy-B, would have acceptable corrosion resistance in molten fluoride salts; however, this alloy has limitations, specifically that it exhibits brittleness after service between 650 °C and 815 °C and shows poor air oxidation resistance. Hastelloy-N was designed to obtain the molten salt corrosion resistance of Hastelloy-B, but without the effects of extensive oxidation and embrittlement. However, Hastelloy-N lacks the high temperature strength of the other Ni and Fe–Ni-based alloys tested.

From the thermodynamics exhibited in Fig. 1, any corrosion of a Ni or Fe-based alloy in a pure molten alkali fluoride salt could be expected to be minimal because the main salt constituents are more stable than any potential corrosion product. However, anions of molten salts such as fluoride ions can lead to increased corrosion rates if they can form stable complex ions with metals such as Cr and Fe [6]. CrF_2 and FeF_2 are examples of Lewis acids in molten fluorides. These acids would interact with a Lewis base, F^-, forming complexes such as $[CrF_4]^{2-}$ and $[FeF_4]^{2-}$, that stabilize the acidic component and decrease the chemical activity [8]. It has been

* Corresponding author. Tel.: +1 608 263 2953; fax: +1 608 263 7451.
E-mail address: lolson@wisc.edu (L.C. Olson).

0022-1139/$ – see front matter © 2008 Elsevier B.V.Elsevier B.V. All rights reserved.
doi:10.1016/j.jfluchem.2008.05.008

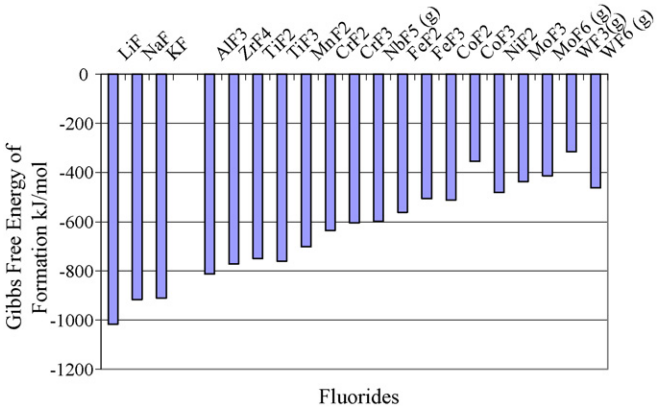

Fig. 1. Gibbs free energy of formation per molecule of F_2 for the salt constituents and the metal fluorides formed from the tested alloys at 850 °C. The Gibbs free energy of formation data in the graph was calculated using HSC Chemistry 5.11 computer software and its associated databases.

Table 1
Properties of molten FLiNaK salt at 700 °C [1]

Salt	FLiNaK
Melting point (°C)	454
Boiling point (°C)	1570
Density (g/cm^3)	2.02
Heat capacity (J/g °C)	1.88
Viscosity (cP)	2.9
Thermal conductivity (W/m K)	0.92

reported for LiF–NaF–ZrF_4 that as the basicity of the melt increases (by decreasing the amount of ZrF_4), the Cr^{3+}/Cr^{2+} cation ratio increases [9]. Pure FLiNaK, a ternary eutectic salt consisting of LiF, NaF, and KF (LiF–NaF–KF: 46.5–11.5–42 mol%), is known to be a strongly basic solvent that tends to stabilize the Cr^{3+} and Fe^{3+} valence states, and the primary valence state of Cr metal in FLiNaK is Cr^{3+} [8].

Because previous corrosion testing at Oak Ridge National Laboratory (ORNL) was primarily concerned with lower temperatures (about 650 °C) and refining Hastelloy-N [8] and NASA's corrosion testing occurred about 30 °C higher than their fluoride salts relatively high melting points (about 770 °C and 910 °C) [2], the present study was undertaken to evaluate the corrosion performance of a number of candidate alloys in FLiNaK salt at 850 °C. This high test temperature was selected because it approaches the maximum temperature expected on the hot side of a reactor-to-hydrogen-production-plant heat transfer system; the peak helium temperature from the helium cooled high temperature reactor has been estimated to be about 900 °C by ORNL [1]. The alloys tested include Ni-based high temperature alloys, Hastelloy-N, Hastelloy-X, Haynes-230, and Inconel-617, an Fe–Ni-based alloy Incoloy-800H, Ni-201 a nearly pure Ni alloy with minor alloying additions, and a refractory alloy Nb–1Zr.

2. Experimental

FLiNaK was selected for this research, based on a recent analysis [1] that identified this salt to be among the leading salts considered from the standpoint of turbulent heat transfer as well as having a low vapor pressure at the envisioned peak operating temperature (~0.2 mm Hg at 850 °C) [1]. Important thermal properties of FLiNaK are listed in Table 1. FLiNaK salt, purified by sparging with an argon H_2/HF followed by a H_2 gas mixture, was procured from Electrochemical Systems Inc., in Oak Ridge, TN, USA. This purification process removed residual water and oxygen from the melt and minimized metal impurities. Inductively Coupled Plasma-Atomic Emission Spectroscopy (ICP-AES) analysis performed on a sample of the salt prior to testing detected the following impurities: 44 ppm Ca, 22 ppm Fe, 7 ppm B, 5 ppm Cr, 5 ppm Cu, and 5 ppm Ni; other elements were determined to be either below 5 ppm or below the quantitative detection limits of ICP-AES. Impurities present in the FLiNaK can dramatically influence corrosion. For example, water present in the initial salt can lead to dramatically increased corrosion through the production of HF [2]. However, for the present study, the effects of trace impurities on corrosion were not specifically investigated in order to maintain focus on the broader goals of comparing the relative corrosion performance of various alloys. Future electrochemical tests are planned in which Zr metal will be added to the salt to act as a reducing agent to suppress the solubility of alloying constituents. Zr metal has been used in LiF–BeF_2–ZrF_4 to reduce impurities as reported by Jenkins [10] and to adjust the U^{4+}/U^{3+} ratio as reported by ORNL [11].

Table 2 lists the compositions of the alloys tested in this study. The alloys were selected based on their high temperature strength, code certification status, and their history of prior usage in high temperature applications. An exception was Ni-201, a nearly pure Ni alloy with minor alloying additions that was selected based on the remarkably high corrosion resistance of Ni in molten fluoride salts. A refractory alloy Nb–1Zr was also tested because of its inherently high melting point and previous work [2] that indicated it should resist corrosion.

Corrosion tests were performed in graphite capsules because of the expected relative inertness of graphite to molten fluoride salts [6]. Some previous studies [12,13] have used similar materials for test containers and test samples. This is ideal; however, to minimize cost graphite was selected as the container material for all test samples in this study. Purified graphite, grade AXZ-5Q1 was obtained from POCO Graphite Inc. This POCO graphite had an average particle size of 5 μm and a pore size of 0.7 μm [14]. Previous studies have shown that small pore sizes are desirable from the standpoint of minimizing salt infiltration into the graphite [15]. The graphite was machined into crucibles, crucible lids, holding rods, and fixturing screws. Prior to corrosion testing, the graphite crucibles and components were cleaned ultrasonically in methanol and water, to remove contaminants from the machining process, before being heated in an argon environment to 1000 °C for 8 h to remove residual water and oxygen. After the

Table 2
Nominal compositions (wt.%) of the alloys tested in the present study

Alloy	Cr	Mo	W	Al	Ti	Fe	C	Co	Ni	Mn	Nb	Zr
Haynes-230	22.5	1.2	14.1	0.3		1.8	0.1	0.3	59	0.5		
Inconel-617	22.1	9.6		1.1	0.4	1.1	0.1	12.4	52.9	0.1		
Hastelloy-N	6.3	16.1	0.1			4.0		0.2	72.2	0.5		
Hastelloy-X	21.3	8.8	0.4	0.1		19.3	0.1	1.4	47.5	0.5		
Nb–1Zr											99.0	1.0
Incoloy-800H	20.4			0.5	0.6	45.3	0.1		31.6	0.8		
Ni-201						0.1			99.4	0.2		

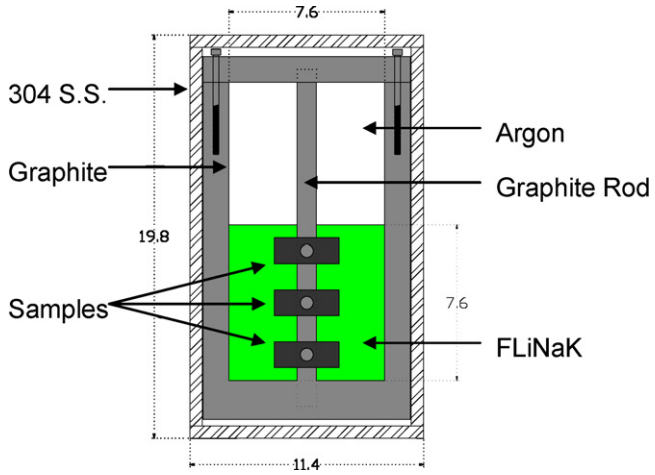

Fig. 2. Schematic illustration of the corrosion capsule apparatus used in the present study for testing corrosion performance of various alloys in molten FLiNaK salt at 850 °C for 500 h. Dimensions are in centimeters.

graphite bake-out, the alloy samples were placed in their corresponding graphite crucibles. Three samples of a given test alloy were fixtured to the central graphite rod using graphite screws. Therefore, all alloys were tested in triplicate, with one crucible being dedicated to each of the alloys. To ensure salt purity, the graphite crucibles were encapsulated in an outer 304 stainless steel containment, and welded shut, leaving a 1/4 in. hole in the stainless steel and graphite crucible lids through which molten FLiNaK salt was introduced. Fig. 2 schematically illustrates the design of the corrosion test capsule.

The FLiNaK salt was pumped into the corrosion capsules from a salt reservoir inside an argon atmosphere glove box as shown in Fig. 3. The mass of salt pumped into the capsules was monitored during pumping and verified by weighing the capsule before and after adding the molten salt. The amount of salt added to each capsule was nominally 0.83 ± 0.16 kg. The variability of the mass was due to the dynamics of the transfer tube system and was not believed to be significant enough to alter the corrosion trends. The volume occupied by the molten salt may be calculated as a function of temperature (in °C) from its density (in units of kg/m^3) using the relationship: $\rho = 2530 - 0.73\,T$ [1].

The final welds to seal the capsules were performed in a furnace inside of the glove box at 600 °C, immediately after being filled with FLiNaK, to lower the capsule's internal pressure at 850 °C. After the final weld, the capsules were placed in an argon atmosphere box furnace, where they were heated up to 850 °C and the salt was maintained at this temperature for 500 h.

Fig. 3. Transfer of molten FLiNaK salt into the corrosion capsule inside a glove box.

After the 500 h exposure, the furnace temperature was lowered to 500 °C and the capsules were inverted to allow the FLiNaK salt to drain away from the alloy samples prior to cooling the experiment to below the melting point of FLiNaK. After the capsules reached room temperature, the corrosion test capsules were cut open using an automated CNC mill. The retrieved samples, were cleaned of residual FLiNaK using 1 M $Al(NO_3)_3$ according to the method used by Kirillov and Fedulov [16]. Following this the samples were evaluated using weight change measurements and scanning electron microscopy. The chemical composition of the salts after corrosion tests was evaluated using ICP-AES.

3. Results and discussion

The results of weight change measurements of the alloys after corrosion testing in molten FLiNaK at 850 °C for 500 h are shown in Fig. 4. For the four Ni-based alloys, Hastelloy-N, Hastelloy-X, Inconel-617, and Haynes-230, the weight-loss due to corrosion was noted to increase with the Cr-content of the alloy. Ni-201, a predominantly Ni-containing alloy with no Cr, was virtually immune to attack. The large variations in weight-loss between the Ni-base alloys and the Fe–Ni-based alloy, all having Cr levels of about 20%, demonstrate the complex roles alloying elements such as Mo, W, Fe, and Co play in corrosion susceptibility. For example, it may be noted that Hastelloy-X and Inconel-617 have similar chemical compositions, except that the Fe in Hastelloy-X is mostly replaced by Co in Inconel-617 and Inconel-617 demonstrated nearly twice the weight-loss per area as Hastelloy-X.

Fig. 5 shows the ICP-AES analysis of Cr-content of the salt after corrosion tests as a function of the Cr-content of the alloy tested in that particular salt. A reasonable correlation exists between the Cr-

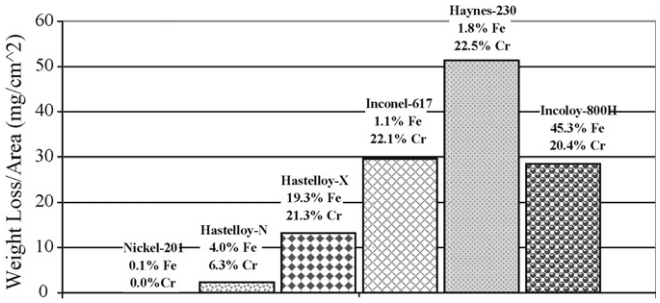

Fig. 4. Weight-loss due to corrosion for various alloys after exposure to FLiNaK at 850 °C for 500 h in graphite capsules.

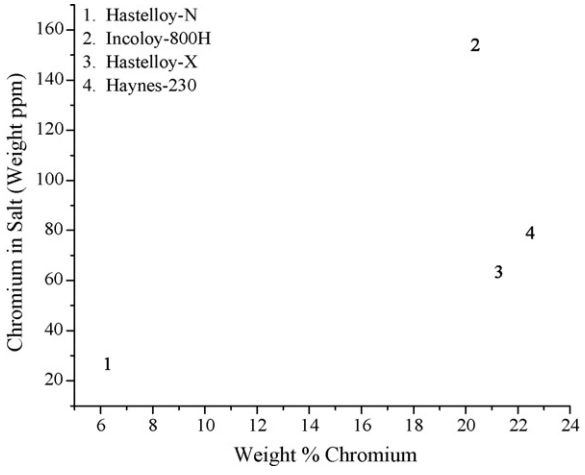

Fig. 5. Cr-content of the salt after corrosion tests as determined by ICP-AES as a function of the Cr-content of the alloy.

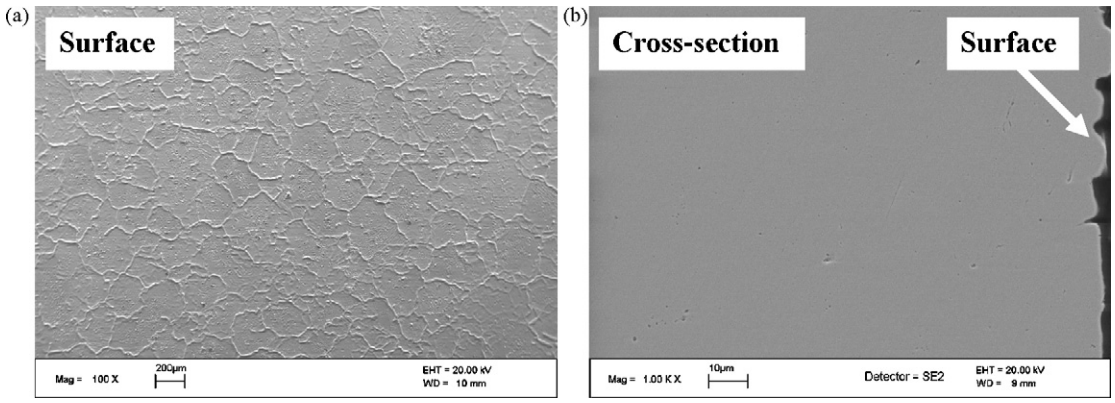

Fig. 6. Scanning electron microscopy images of Ni-201 alloy (unetched) after corrosion testing in FLiNaK at 850 °C for 500 h. (a) Surface plan view and (b) cross-sectional view.

content of the salt and the Cr-content of the alloy for the Ni-based alloys; however a larger amount of Cr was detected from the salt used to test the Fe–Ni-based alloy, Incoloy-800H.

Fig. 6 shows the SEM images of the surface and cross-section of Ni-201 alloy after the corrosion test. With the exception of minor attack at the grain boundaries, this alloy exhibited very little corrosion attack due to the strong resistance of Ni to dissolution in molten fluoride salts.

The corrosion attack was more severe for Hastelloy-N (6.3% Cr) where Cr depletion up to depths of about 50 μm was observed (Fig. 7). EDS X-ray mapping performed on cross-sectional images of this alloy showed a reasonably uniform depletion of Cr (Fig. 8(a)) and the presence of Mo-enriched precipitates at the grain boundaries (Fig. 8(b)), confirming that Mo is generally resistant to dissolution in molten FLiNaK salt.

As shown in Fig. 9, Hastelloy-X (21.3% Cr) exhibited grain boundary attack up to depths of at least 300 μm below the surface. Significant depletion of Cr was noted to have occurred through out the grains, but this depletion was markedly more severe along the grain boundaries. However, there was depletion of Cr in the grains as well, as confirmed by SEM-EDS analysis. As in the case of Hastelloy-N, Mo-rich precipitates at the grain boundaries were observed to remain intact after corrosion tests.

Inconel-617 (22.1% Cr) was uniformly depleted in Cr up to depths of about 100 μm from the surface, and experienced dramatic grain boundary corrosion throughout the thickness of

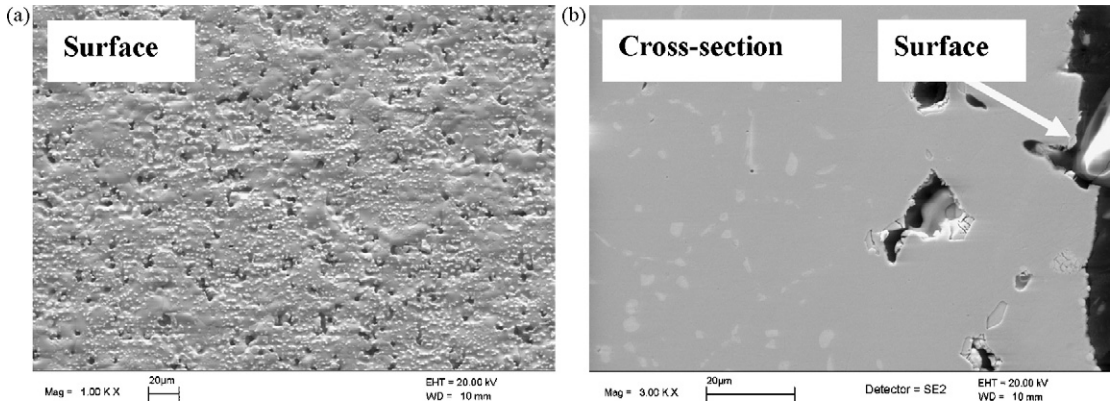

Fig. 7. Scanning electron microscopy images of Hastelloy-N (unetched) after corrosion testing in FLiNaK at 850 °C for 500 h. (a) Surface plan view and (b) cross-sectional view.

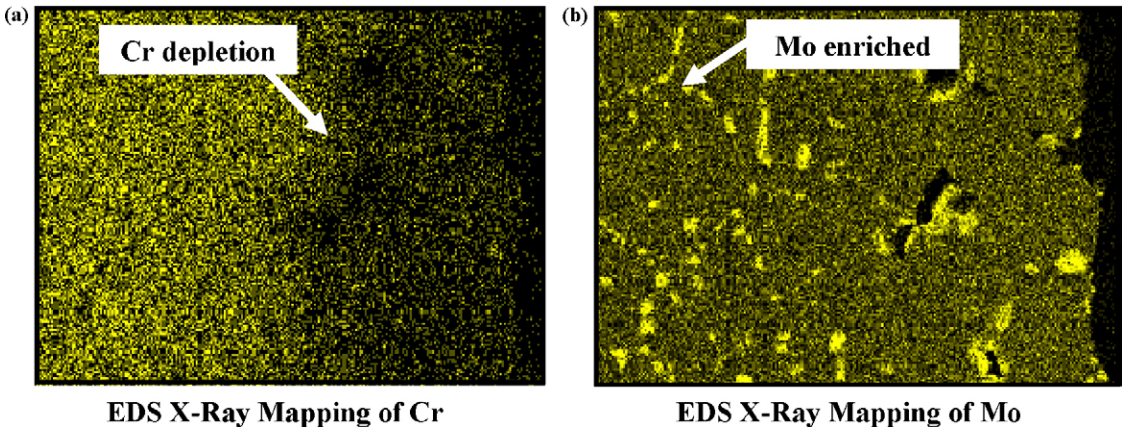

Fig. 8. EDS X-ray maps of cross-sectional images of Hastelloy-N after corrosion testing in FLiNaK at 850 °C for 500 h for (a) Cr and (b) Mo.

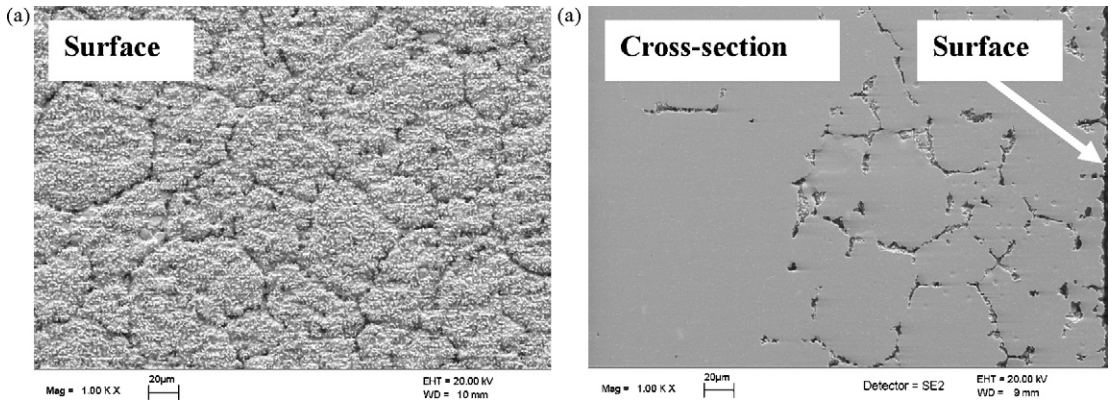

Fig. 9. Scanning electron microscopy images of Hastelloy-X (unetched) after corrosion testing in FLiNaK at 850 °C for 500 h. (a) Surface plan view and (b) cross-sectional view.

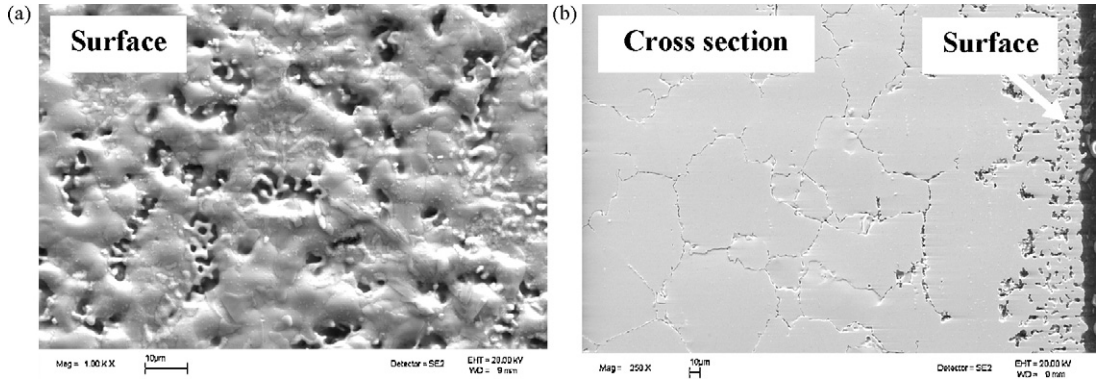

Fig. 10. Scanning electron microscopy images of Inconel-617 (unetched) after corrosion testing in FLiNaK at 850 °C for 500 h. (a) Surface plan view and (b) cross-sectional view.

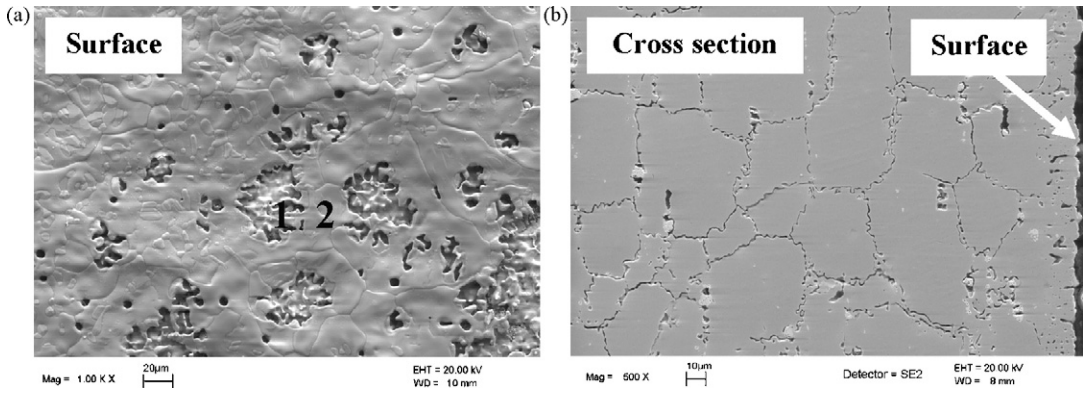

Fig. 11. Scanning electron microscopy images of Haynes-230 (unetched) after corrosion testing in FLiNaK at 850 °C for 500 h. (a) Surface plan view and (b) cross-sectional view.

the sample, as shown in Fig. 10. Similar attack was observed for Haynes-230 (22.5% Cr), however the surface of Haynes-230 exhibited a Ni-enriched layer (Fig. 11 and Table 3).

For Haynes-230, W-rich precipitates (Fig. 12) were observed at the grain boundaries due to the relatively high W content of this alloy, demonstrating that W, like Mo is resistant to attack from molten fluoride salt. The fundamental reason why Haynes-230 experienced more weight-loss than the other high Cr-containing alloys warrants further investigation. As previously mentioned, Cr was expected to be selectively attacked due to the highly negative Gibb's free energy of its fluoride phase so W-rich precipitates being present after such an attack was not surprising. Streicher [17], has shown for several Hastelloy alloys that carbides of the type M_6C and an intermetallic phase $(Ni, Fe, Co)_3(W, Mo, Cr)_2$ formed between 649 and 1204 °C can lead to intergranular corrosion and a galvanic couple between the alloy matrix and the precipitate. It is speculated that a similar effect is occurring with the W-rich precipitate phases formed at the elevated temperatures in the grain boundaries. The formation of a Cr-depleted and Ni-enriched

Table 3
EDS point scans and alloy base data (wt.%)

EDS point	Cr	Fe	Ni	W
1	4.1	2.8	77.4	14.5
2	0.7	1.3	87.3	0.0
Haynes-230 Heat Data	22.5	1.8	58.7	14.1

Points correspond to numbers in Fig. 11.

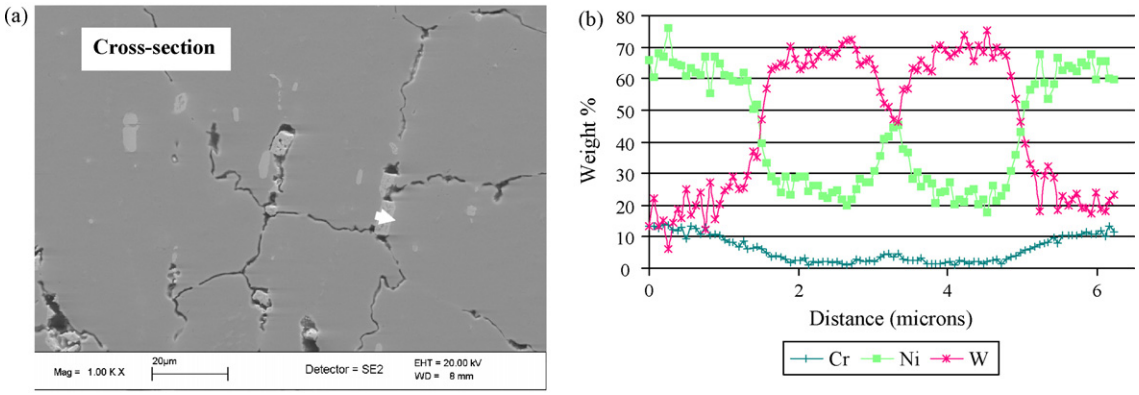

Fig. 12. Grain boundary corrosion showing the presence of W-rich precipitates at the grain boundaries in unetched Haynes-230. (a) Enlarged view of cross-section viewed in Fig. 11 and (b) line scan over the precipitate indicated with the white arrow in (a).

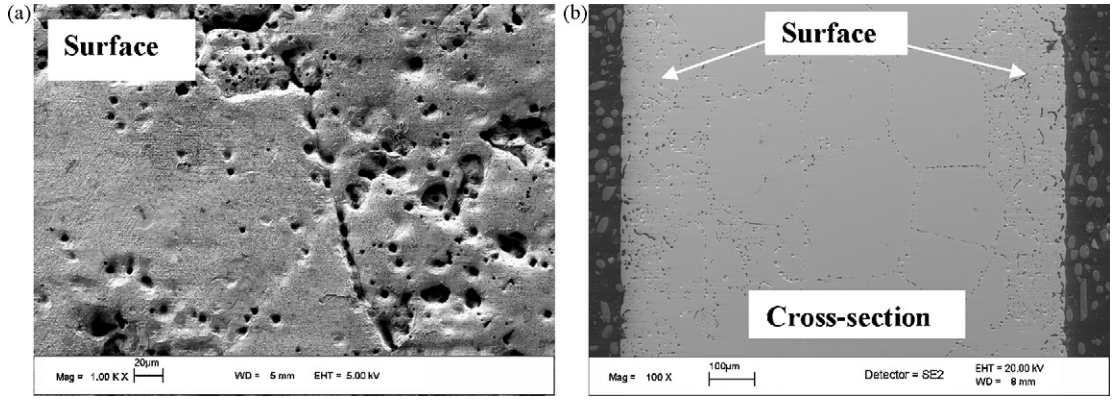

Fig. 13. Scanning electron micrograph (a) showing pits on the surface of Incoloy-800H after corrosion tests and (b) cross-sectional view showing grain boundary attack.

surface layer present on the Haynes-230 samples may eventually limit the overall dissolution rate of Cr from the alloy.

The Cr dealloying for the Fe–Ni-based Incoloy-800H (20.4% Cr) appeared to result in pitting of the surface. An SEM micrograph of the pitted surface of Incoloy-800H samples is shown in Fig. 13. As in the case of previous alloys, severe depletion of Cr was observed particularly along the grain boundaries and this effect was more pronounced for smaller grains compared to the larger grains. Furthermore, the thermal effects of exposing this alloy at 850 °C for 500 h leads to the formation of Cr-carbide at the grain boundaries and this Cr is readily diffused into the salt along the grain boundaries. EDS analysis shows the Cr depleted region, extends into the surface about 150 μm.

It is clear from the weight-loss measurements and significant Cr depletion that the graphite crucible and components might have played a role in accelerating the corrosion of the alloys. This possible graphite interaction has been further established in our recent experiments where corrosion testing of Incoloy-800H samples in an Incoloy-800H crucible, under identical conditions, showed significantly less corrosion than the Incoloy-800H tested in the graphite crucibles. It has been known for some time that graphite containers can lead to accelerated corrosion of alloys exposed to molten salts by what Ozeryanaya [18] called non-electric transfer [18]. It is believed that an acceleration of corrosion or other graphite–alloy interaction within the corrosion capsules was promoted by FLiNaK's tendency to sustain multiple valence states of Cr and the difference in chemical activity between the electronegative metal Cr in the alloy and that of the graphite crucible and components. A Cr rich film was detected on the graphite rod used to hold the Incoloy-800H samples, and X-ray diffraction analysis of the film indicated Cr_7C_3. This Cr-carbide film formation is speculated to be the result of the reaction, $21CrF_2 + 3C \rightarrow Cr_7C_3 + 14CrF_3$ at the graphite surface for the graphite capsule used to test Incoloy-800H, similar to the reactions

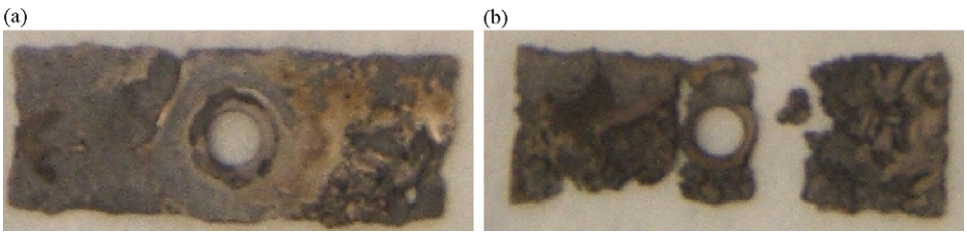

Fig. 14. Photographs of the Nb–1Zr alloy after corrosion tests showing severe corrosion and embrittlement. (a) Shows general corrosion and (b) demonstrates the effect of the embrittlement on the alloy.

seen in molten salt heat treatment baths discussed by Ozeryanaya [18]. Following the further oxidation of Cr^{2+} to Cr^{3+} and formation of the Cr-carbide at the graphite interface, the Cr^{3+} ion migrates back to the alloy surface through convection or diffusion where it oxidizes Cr metal in the alloy and reduces back to Cr^{2+} from Cr^{3+} according to the reaction, $2CrF_3 + Cr \rightarrow 3CrF_2$ [18]. A detailed analysis of Cr–graphite interactions will be published in future work. EMF measurements to determine the relative corrosion potentials of the alloys and graphite in molten FLiNaK environment are required to further support and establish this mechanism. These measurements are presently being undertaken and the results will be presented in a future paper.

Nb–1Zr appeared to have been especially effected by a graphite–alloy interaction that led to severe embrittlement (Fig. 14). Zr can be expected to be more reactive in molten fluoride salts than most other alloying constituents, as shown in Fig. 1, and surmised from its previously mentioned use as a reducing agent. Zr is more electronegative than Cr and known to react with graphite in molten salts by the same non-electric transfer mechanism as discussed for Cr previously, which results in the formation of ZrC [18], and Nb and its alloys are also known to be embrittled by low levels of impurities such as carbon [19].

4. Conclusion

A number of potential high temperature alloys and alloy Ni-201 were evaluated for corrosion in molten FLiNaK salt at 850 °C for exposure durations of 500 h, using graphite crucibles encapsulated in stainless steel containments to ensure salt purity. In the Cr-containing alloys the dissolution of Cr into the molten salt was observed, an effect that was particularly pronounced at the grain boundaries of the alloys. The Cr-content of the salt after corrosion tests generally correlated with the Cr-content of the corresponding alloy. The Ni-201 alloy, which is predominantly Ni with minor alloying additions, was resistant to corrosion. The refractory alloy Nb–1Zr exhibited severe corrosion and embrittlement. The graphite crucible appears to have accelerated the corrosion process, by way of forming Cr-carbide phases for the Cr-containing alloys and a Zr-carbide phase for the Nb–1Zr alloy. The enhanced corrosion rate induced by the graphite crucible and components provides an accelerated environment for evaluating the relative corrosion performance of various candidate alloys.

Acknowledgements

The authors would like to acknowledge the assistance of Dr. Dane Wilson and Dr. Dave Williams at Oak Ridge National Laboratory in this research. This research is being supported by United States DoE Grant No. DOE-FC07-05ID14675.

References

[1] D.F. Williams, Assessment of Candidate Molten Salt Coolants for the NGNP/NHI Heat-Transfer Loop, ORNL/TM-2006/69, 2006, pp. 1–44.
[2] A.K. Misra, J.D. Whittenberger, in: Proceedings of the 22nd Intersociety Energy Conversion Engineering Conference cosponsored by the AIAA ANS ASME SAE IEEE ACS and AIChE Philadelphia, PA, 10–14 August, 1987, AIAA-87-9226.
[3] C. Forsberg, P. Peterson, H. Zhao, J. Solar Energy Eng. 129 (2007) 141–146.
[4] W. Manly, J. Coobs, J. DeVan, D. Douglas, H. Inouye, P. Patriarca, T. Roche, J. Scott, in: R. Hurst, R.N. Lyon, C.M. Nicholls (Eds.), Progress in Nuclear Energy, Series IV: Technology, Engineering and Safety, vol. 2, Pergamon Press, New York, 1960, pp. 164–179.
[5] J. Steinmetz, P. Steinmetz, A. Huntz, Solid State Phenom. 21/22 (1992) 223–276.
[6] D. Williams, D. Wilson, J. Keiser, L. Toth, J. Caja, Proceedings of Global 2003, Embedded Topical in 2003 American Nuclear Society Winter Meeting, New Orleans, LA, 16–20 November 2003, Session 2A: Coolant/Material Interactions in Advanced Reactor Systems, Research on Molten Fluorides as High Temperature Heat Transfer Agents.
[7] J. Koger, in: S. Cramer, B. Covino (Eds.), ASM Handbook: Corrosion: Fundamentals, Testing, and Protection, vol. 13A, ASM International, OH, 2003, pp. 124–128.
[8] D. Williams, L. Toth, K. Clarno, Assessment of Candidate Molten Salt Coolants for the Advanced High-Temperature Reactor (AHTR), ORNL/TM-2006/12, 2006, pp. 1–69.
[9] J. Redman, Effect of Fuel Composition on the Equilibria $3CrF_2 \leftrightarrow 2CrF_3 + Cr^0$ and $3FeF_2 \leftrightarrow 2FeF_3 + Fe^0$, in: H. MacPherson (Ed.) Molten Salt Reactor Quarterly Progress Report, ORNL-2626, 1959, pp. 95–96.
[10] H. Jenkins, Electrochemical Measurements in Molten Fluorides, The University of Tennessee, Analytical Chemistry, PhD Dissertation, pp. 29.
[11] D. Manning, F. Clayton, Reference electrode studies in molten fluorides, in: M. Rosenthal, R. Briggs, P. Haubenreich (Ed.) Molten-Salt Reactor Program Semi-annual Progress Report, ORNL-4622, 1971, pp. 115.
[12] J. Koger, A. Litman, Compatibility of Molybdenum-base Alloy TZM with LiF–BeF_2–ThF_4–UF_4 (68–20–11.7–0.3 mole%) at 1100 °C, ORNL-TM-2724, 1969, pp. 1–14.
[13] J. Whittenberger, J. Mater. Eng. Perform. 3 (1994) 763–774.
[14] POCO Inc., AXZ-5Q, URL: http://www.poco.com/MaterialsandServices/Graphite/IndustrialGrades/AXZ5Q/tabid/92/Default.aspx
[15] H. McKoy, R. Beatty, W. Cook, R. Gehlbach, C. Kennedy, J. Koger, A. Litman, C. Sessions, J. Weir, Nucl. Appl. Technol. 8 (1970) 156–169.
[16] V. Kirillov, V. Fedulov, Fiziko-Khim. Mekhanika Mater. 16 (1980) 22–25.
[17] M. Streicher, Corrosion-NACE 32 (1976) 79–93.
[18] I. Ozeryanaya, Met. Sci. Heat Treat. 3 (1985) 184–188.
[19] J. Shields, J. Dahl, in: S. Lampman, T. Zorc (Eds.), ASM Handbook: Heat Treating, vol. 4, ASM International, OH, 1991, pp. 815–819.